Chemical Science

Accepted Manuscript

This article can be cited before page numbers have been issued, to do this please use: E. Sutcliffe, J. P. Aalto and R. G. Hadt, *Chem. Sci.*, 2026, DOI: 10.1039/D6SC04497B.

ROYAL SOCIETY OF CHEMISTRY

rsc.li/chemical-science

Excited-state orbital angular momentum enables all-optical molecular spin coherence

Erica Sutcliffe,† Jonathan P. Aalto,† Ryan G. Hadt*

Division of Chemistry and Chemical Engineering, Arthur Amos Noyes Laboratory of Chemical Physics, California Institute of Technology, Pasadena, California 91125, United States

†*Authors contributed equally.*

**Corresponding author: rghadt@caltech.edu*

Abstract

Paramagnetic molecules are promising quantum sensors with dimensions and environmental compatibility inaccessible to solid-state defects. Realizing this promise, however, requires optical methods for initializing and reading out coherent spin dynamics. Ultrafast pump–probe polarization spectroscopy provides such a route, but previous demonstrations have relied on high-symmetry complexes in which ground-state orbital angular momentum enables spin–photon coupling. Here we demonstrate the first ultrafast spin coherence measurements on non-octahedral molecules and show that excited-state orbital angular momentum can instead provide the optical interface in axial tungsten(V)-oxo complexes. Circularly polarized excitation generates room-temperature spin coherence that persists for several nanoseconds, enabling time-domain optical detection of electron paramagnetic resonance (EPR) spectra, including *g* value anisotropy in a polymer matrix, and solution-phase DC magnetic field detection down to 5 mT. This work establishes a route to ultrafast, all-optical spin spectroscopy and quantum sensing in lower-symmetry, chemically tunable coordination complexes.

Introduction

Molecular quantum sensing utilizes the electron spin as a quantum bit (qubit) to enable next-generation sensing modalities.[1–4] The small size and synthetic tunability of molecules render them especially suitable for *in situ* microscopy relative to nitrogen-vacancy centers and other solid-state architectures,[5,6] but such applications have heretofore remained elusive due to the lack of optical readout mechanisms and short coherence times, T_2^*. Our group has aimed to address these drawbacks through the development of time-resolved Faraday ellipticity/rotation (TRFE/R), an ultrafast, all-optical approach to measure electron spin decoherence in the femto-to-nanosecond regime.[7,8] With several orders of magnitude improvement in both temporal and spatial resolution over typical microwave techniques, TRFE/R has shown promise in elucidating the few-picosecond spin dynamics of octahedral (O_h) iridium(IV) complexes in aqueous solutions at room temperature.[7,8] In contrast, the fast decoherence of these complexes renders them microwave addressable only at very low temperatures. Optical addressability is achieved with a circularly polarized pump pulse to generate a spin-polarized ensemble of molecules, the decoherence of which is measured through the change in optical polarization of a subsequent probe pulse. Analysis of aqueous solutions and polymer films has highlighted the operative role of molecular tumbling as a primary driver of picosecond decoherence in $[IrX_6]^{2-}$ (X = Cl, Br). In addition to providing information on decoherence, TRFE enables all-optical detection of the molecular electronic *g* value—a highly informative magnetic resonance parameter—from free induction decays measured in a perpendicular magnetic field.

At present, a key limitation of TRFE/R is the dearth of molecular systems with suitable spin–photon coupling. Spin polarization induced by absorption of a circularly polarized photon is made possible through spin–orbit coupling (SOC) and orbital angular momentum (OAM), which presents a challenge in transition-metal complexes since the ligand field typically quenches the OAM of *d* electrons. However, this challenge can be overcome through judicious design of the coordination environment. In $[IrX_6]^{2-}$, the low-spin O_h d^5 electronic structure leads to a triply orbital degenerate $^2T_{2g}$ ground state (GS) formed from the $\{d_{xy},d_{yz},d_{xz}\}$ orbitals (**Figure 1A**). These orbitals are related by 90° rotations about x, y, and z, representing an eigenstate of the OAM operators with effective (residual) OAM of $L' = 1$. Through the efficient spin–photon interaction afforded by this large OAM, spin dynamics can be initialized and read-out optically even at few-micromolar Ir(IV) concentrations.[7] However, $^2T_{2g}$ GSs require high-symmetry molecules, limiting the potential to connect to the rich geometric and electronic structures of coordination complexes. Large GS SOC and OAM also drive spin decoherence,[9–11] resulting in the picosecond T_2^* observed for $[IrX_6]^{2-}$. Thus, establishing TRFE/R addressability in lower-symmetry systems represents a critical step toward expanding ultrafast, all-optical spin coherence spectroscopy across paramagnetic transition metals ranging from metallaphotoredox catalysts to metalloenzyme active sites.

One avenue to circumvent these issues is to utilize OAM in the excited state (ES). Such a mechanism was recently proposed by the Transue group for optically induced magnetization in a pseudo-C_{4v},d^1 complex $[Na(THF)_6][WO(ODipp)_4]$ (**Figure 1A**, complex **1**).[12] This work provided detailed spectroscopic characterization

View Article Online
DOI: 10.1039/B6SC04497B

using magnetic circular dichroism (MCD) and electron paramagnetic resonance (EPR), predicting strong GS spin polarization via circularly polarized excitation. However, direct measurements of optically induced spin polarization, including ultrafast spin decoherence measurements, have yet to be made.

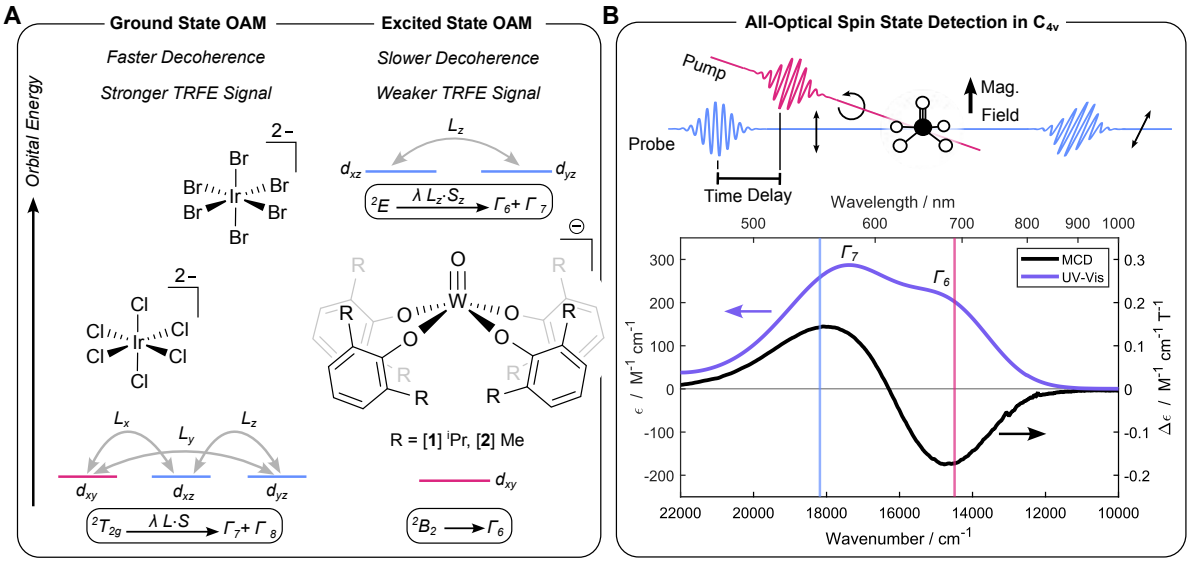

Figure 1. Relationship between OAM and spin dynamics. **A** *Origins of GS and ES OAM.* **B** *Schematic of all-optical spin detection (top). Room-temperature electronic absorption and MCD spectra of **1** in THF (bottom); vertical lines represent pump (red) and probe (blue) wavelengths.*

Descent in symmetry from O_h to C_{4v} lifts the triple degeneracy of the t_{2g} orbitals, which results in a $^2B_2$ (Γ_6) GS (d_{xy}) and a ^2E ES (d_{xz}/d_{yz}). The d orbitals of the ^2E state are eigenstates of the L_z operator, as they are related through a 90° rotation about the z axis, leading to modest ES OAM and SOC within the Γ_6 and Γ_7 states ($\lambda = \zeta_{W(V)} \approx 3500\ cm^{-1}$).[13] MCD spectroscopy displays a clear signature of the ^2E ES, with the two spin-orbit states showing intense, oppositely-signed bands forming a derivative-like shape—a pseudo-*A* term.[14,15] Such line-shape is characteristic of degenerate (or nearly-degenerate) ES orbital manifolds related via rotation about a mutually orthogonal axis and indicates non-negligible ES OAM, rendering **1** an ideal candidate to test whether ES OAM may be leveraged for TRFE/R spectroscopy in axial systems.

Here we demonstrate nanosecond-scale spin coherence in room-temperature solutions of **1**, including record sensitivities to DC magnetic fields. We further probe environmental factors to elucidate the mechanism of decoherence and demonstrate all-optically detected EPR spectroscopy.

Results

To test the excited-state OAM hypothesis and optically access the spin dynamics of **1** (11 mM in THF), we photoexcite between 680 – 700 nm ($\Gamma_6 \rightarrow \Gamma_6$) and probe the TRFE/R response at 550 nm ($\Gamma_6 \rightarrow \Gamma_7$). These pump/probe wavelengths reside within the steady state MCD pseudo-*A* term (**Figure 1**). Room-temperature TRFR measurements reveal a signal persisting for several nanoseconds (**Figure 2A**), orders of magnitude longer than high-symmetry Ir(IV) complexes.[7,8] Application of a perpendicular magnetic field (0.39 T for consistency with EPR) induces a clear free induction decay (**Figure 2B**), demonstrating that the long-lived signal corresponds to spin polarization. Damped cosine fitting reveals $g_{iso} = 1.76$, consistent with the continuous-wave (CW) EPR spectrum at 77 K in 2-MeTHF (**Figure S4**, $g_{iso} = (g_{\parallel} + 2g_{\perp}) = 1.772$). Thus, this represents the first measurement of ultrafast electron spin coherence in a non-O_h molecule.

View Article Online
DOI: 10.1039/D6SC04497B

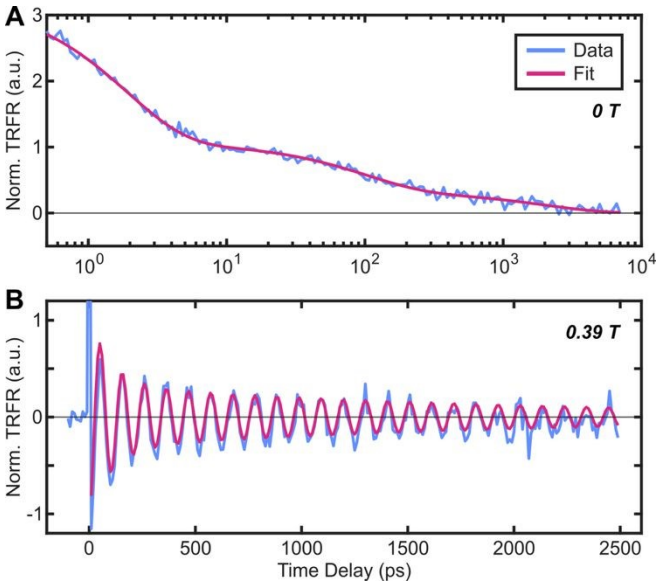

Figure 2. Ultrafast spin dynamics of 1. A *Decoherence at 0 T.* **B** *Free induction decay at 0.39 T. Fit to both consists of a triexponential decoherence rate multiplied by a cosine at the Larmor frequency (0 Hz for* **A***).*

The 0 T decoherence profile fits well to a tri-exponential decay with time constants $\tau_1 = 1.9(1)$ ps, $\tau_2 = 100(16)$ ps and $\tau_3 = 2.0(5)$ ns (error estimated from least-squared fit). Predictably, the signal intensity is noticeably weaker than $[IrX_6]^{2-}$ due to reduced OAM, limiting the accuracy of the fitted time constants. Beyond the intensity, the fit itself contrasts with the purely monoexponential decays observed in $[IrX_6]^{2-}$ and the stretched exponentials common in pulse EPR. To determine the origin of these components, we carried out further TRFE/R spectral characterization at 0 T (**Figure S39**). With 550 nm probe, TRFE/R give identical traces, albeit with a larger intensity for the former. With a 500 nm probe, the 1.9 ps component switches sign relative to the other two, and no change in this initial component is observed in an applied magnetic field (**Figure S40**), unlike τ_2 and τ_3. Thus, τ_1 is not related to spin dynamics, and subsequent analyses focus on the >10 ps time regime, where only GS spin coherence is present. Transient absorption spectroscopy reveals a short electronic lifetime similar to τ_1, suggesting a potential ES origin for the artefact (**Figure S41**).

Across a variety of molecular qubit systems, the spin-lattice relaxation rate ($1/T_1$) imposes an upper limit on decoherence and is proportional to the amount of residual GS OAM.[11,16,17] Consequently, X-band pulse EPR T_1 values for $[IrBr_6]^{2-}$, obtained via inversion recovery echo sequences at g_{iso} in 3:2 water:glycerol, are short and exceed the EPR detection limit (~100 ns) above 20 K (**Figure 3**, blue).[8] By contrast, pulse EPR of **1** in glassy 2-MeTHF at $g_{\parallel}$ (0.40 T) reveals measurable T_1 values up to 70 K (**Figure 3**, purple), remaining 10–100 times longer than $[IrBr_6]^{2-}$ at temperatures where direct comparison is possible. Similar T_1 behavior is observed at $g_{\perp}$ (0.38 T) (**Figure S11**). Extrapolation of T_1 to room temperature yields qualitative agreement with the observed disparity in TRFR decay rates. For both complexes, the spin-spin decoherence times measured via Hahn echo sequences (T_m) become T_1-limited at higher temperatures, though this does not necessarily mean T_2^* is dictated solely by T_1 in room-temperature solutions. Unlike T_2^*, T_m is insensitive to static inhomogeneity, but both are still subject to spectral diffusion and slow dynamic noise and so are approximations of the true spin-spin decoherence time T_2. In $[IrBr_6]^{2-}$, for instance, immobilization in a polymer matrix extended T_2^* by an order of magnitude relative to aqueous solution, while viscous water:glycerol solutions displayed intermediate decoherence rates. This suggests the question of whether room-temperature decoherence in **1** is similarly suppressed below the T_1 limit by molecular tumbling or other means.

View Article Online
DOI: 10.1039/D6SC04497B

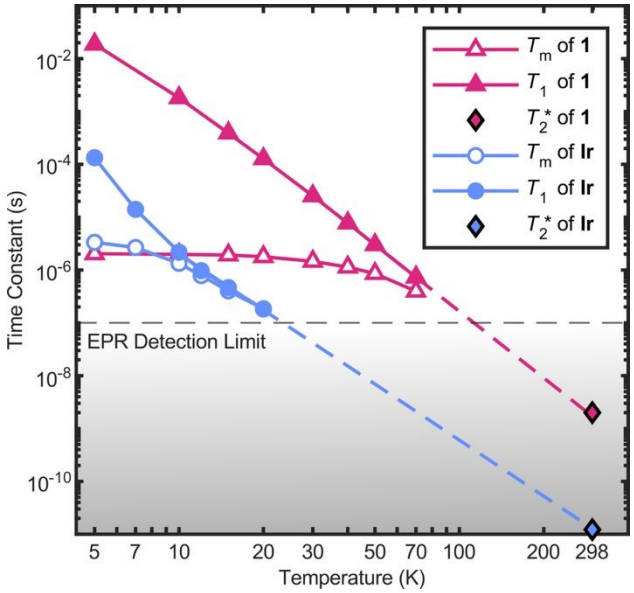

Figure 3. Temperature-dependent spin dynamics. *Pulse EPR (403.2 mT) and TRFR (longest component) measurements for $[IrBr_6]^{2-}$ in 3:2 H_2O:glycerol* [8] *and* ***1*** *in 2-MeTHF (pulse EPR) or THF (TRFR).*

Having demonstrated TRFR addressability in **1**, we sought to elucidate the mechanisms underlying decoherence. While these are increasingly well understood on timescales accessible by pulse EPR, there is little experimental evidence detailing sub-nanosecond decoherence mechanisms in solution. To investigate the impact of molecular tumbling on the observed T_2^* in **1**, polystyrene was added to the THF solution to raise the bulk viscosity from an estimated 0.48 cP to ~13 cP.[18] No change in T_2^* was observed (**Figure S42**). However, this could be due to polystyrene modulating only the bulk viscosity while minimally altering the THF solvation sphere directly surrounding the molecule. The chemical sensitivity of the complex currently precludes the use of other viscous small molecules, such as glycerol, to raise the microscopic viscosity.

With $T_2^* > 1$ ns, diffusion-mediated dipole-dipole interactions between electron spins could lead to decoherence. Indeed, the low-temperature pulse EPR shows a decrease in T_m with concentration (**Figures S12, S13**). However, no change in T_2^* could be detected above noise at room temperature across a four-fold increase in concentration (**Figure S43**).

Hyperfine interactions between the electron spin and adjacent nuclear spins can lead to decoherence, especially with the large gyromagnetic ratio of ^{1}H atoms.[19,20] To address this, deuterated THF was used to remove protons from solvation. However, no change in T_2^* was observed (**Figure S44**). This lack of spin-interaction with solvation is unsurprising given the large steric bulk of the molecule likely providing significant shielding. However, the proton-rich 2,6-diisopropylphenoxide (ODipp) ligands raise the possibility of interaction with proximal nuclear spins. To reduce the number of W-adjacent protons, we replaced the ODipp with 2,6-dimethylphenoxide (ODmp) to form complex **2** (**Figure 1A, SI Section 7**). This caused a slight blueshift of the electronic transitions (**Figure S1**), likely due to the reduced steric bulk causing a slight contraction of the W–O bonds, but the electronic structure remained broadly the same. Despite this structural modification and associated changes to low-temperature decoherence (**Figures S14, S15**), the room-temperature spin dynamics are identical (within noise) to that of **1** (**Figure S45**).

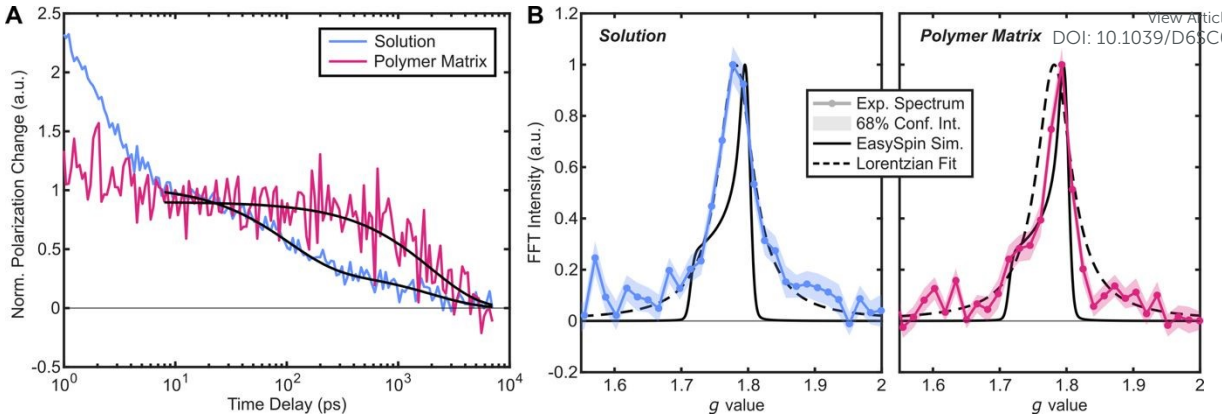

Figure 4. Effect of immobilization on spin dynamics. A *Decoherence at 0 T for* ***1*** *in 11 mM THF solution and a PMMA polymer matrix using TRFR and TRFE, respectively.* **B** *Ultrafast, all-optical EPR spectra at 5 T for solution and film, error bounds given by standard error on mean. A linear background was subtracted from the spectra to aid comparison to the simulation.*

Given the solution-phase nature of these measurements, the solvent itself provides a means to tune the local chemical environment. Butyronitrile has the same viscosity as THF but a significantly larger dielectric constant. However, T_2^* of **1** is not sensitive to solvent dielectric and does not change significantly in any other solvent tested (**Figure S46**).

We further sought to reduce molecular tumbling by encapsulating **1** in a polymethylmethacrylate (PMMA) matrix. This thin-film sample also has a relatively high effective concentration, which suppresses T_m at low temperature (**Figures S12, S13**). The CW EPR and electronic absorption spectra remain largely unchanged (**Figures S2, S7**), however, aside from modest peak broadening, indicating that the electronic structure is mostly preserved.

At 0 T, the room-temperature thin film exhibits significantly different spin dynamics than the solution-phase sample. In particular, the ~100 ps decay component is absent, and the film data are well described by a single exponential with a time constant of ~2 ns, matching the slowest component of the solution-phase decay.

At 5 T, both the solution and polymer-matrix samples exhibit long-lived free induction decays, although the noise level prevents reliable time-domain fitting (**Figure S48**). The Fourier transform, however, reveals the spectral information enabled by the long T_2^* and a narrow EPR linewidth (**Figure 4B, C**). For freely rotating molecules in solution, with their rotational correlation time $\tau_c \ll T_2^*$, a Lorentzian lineshape centered on the isotropic g value is expected. This is exactly what is observed for **1** in THF: a Lorentzian fit reproduces the spectrum almost perfectly, yielding g_{iso} = 1.78, and the linewidth corresponds to $T_2^* \approx 450$ ps.

By contrast, the thin-film spectrum exhibits additional structure and is poorly described by a Lorentzian lineshape. Using spin Hamiltonian parameters obtained from EasySpin simulations of the axial 77 K CW EPR spectrum (**Figure S6, Table S8**), we simulated the expected 5 T spectrum for a frozen solution.[21] The simulated and experimental lineshapes show clear correspondence: the sharp maximum at 1.80 aligns with $g_\perp$, and the shoulder at 1.71 matches $g_\parallel$. Although noise prevents quantitative fitting, and some discrepancy is expected because the spin Hamiltonian can be slightly perturbed across such a large temperature range, the overall agreement is clear.

These results show that g-value anisotropy can be observed all-optically in the time domain at room temperature, even when T_2^* remains several orders of magnitude below the sensitivity limit of pulse EPR. Optically detected g-value anisotropy has previously been reported in bulk $CuSO_4$•$5H_2O$ using magnetic THz dichroism,[22] but the weak absorption cross section for THz magnetic dipole transitions makes this approach less attractive for sensing than TRFE/R.

View Article Online
DOI: 10.1039/D6SC04497B

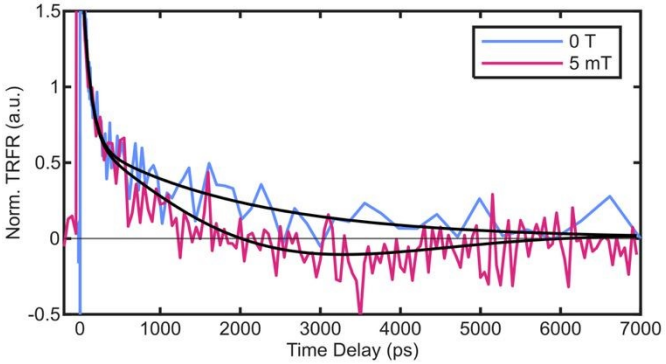

Figure 5. Ultrafast DC magnetic field sensing. *Free induction decay for room temperature solution of **1** under 5 mT applied field.*

Finally, motivated by the environmental robustness of T_2^*, we tested the limit of time-domain DC magnetic field sensing in solution-phase **1**. Fields as low as 5 mT are readily detected (**Figure 5**); even smaller changes may be measurable with an appropriate bias field. To our knowledge, this represents the best DC magnetic-field sensitivity yet reported for a molecule that does not rely on a radical pair mechanism.[23]

Discussion

Room-temperature electron spin decoherence in **1** is biexponential and remains unchanged with spin concentration, solvent dielectric, solvent deuteration, and the number of ligand protons. Immobilization in a polymer matrix removes the fast 100 ps decay component while leaving the slower ~2 ns component unchanged. Because molecular tumbling and spin-spin interactions primarily affect T_2, these results instead point to T_1-limited decoherence for the ~2 ns component, consistent with the convergence of T_1 and T_m in **Figure 3**. This behavior differs from that of the $[IrX_6]^{2-}$ and $[Cu(H_2O)_6]^{2+}$ complexes previously studied with TRFE, where decoherence is also driven by molecular tumbling and spin-spin interactions, respectively.[7,8,24] The environmental insensitivity of T_2^*, together with the strong temperature dependence of T_1, also suggests that this qubit may be well suited for temperature sensing and probing ultrafast, light-induced vibrational dynamics, especially given that decoherence can now be measured on the same timescales as vibrational relaxation processes.[25,26]

The disappearance of the ~100 ps component in the film, however, merits further discussion. Because immobilization largely removes molecular tumbling, the two effects are likely linked. In C_{4v}, the $^2B_2 \rightarrow {}^2E$ transition is (x,y)-polarized, so pump and probe absorption should be strongest for molecules aligned favorably with the photon wavevectors. Through this orientational selectivity, the spin-polarized ensemble of molecules generated by the pump pulse will also be anisotropically oriented. This anisotropy should relax to isotropy on the timescale of τ_c. However, because the GS OAM is low, we expect that molecular rotations will only couple weakly to the spins, allowing the spin ensemble to remain polarized during this process. The probe is subject to the same orientational selection rules, so the initially anisotropic ensemble absorbs more strongly than an isotropic one. In the extreme axial limit, the TRFE/R signal, $\eta(t)$, will follow

$$\eta(t) = \left(\frac{2}{3}e^{-t/\tau_c} + \frac{1}{3}\right)e^{-t/T_2^*} \approx \frac{2}{3}e^{-\frac{t}{\tau_c}} + \frac{1}{3}e^{-\frac{t}{T_2^*}}, \qquad \text{if } \tau_c \ll T_2^* \qquad \text{(Eq. 1)}$$

For a fully isotropic distribution, only one third of the molecules are favorably aligned with the light at any given time, producing a decay depending on τ_c. In the polymer matrix, τ_c is significantly prolonged, leading to a monoexponential decay. The orientational selectivity in this complex is likely not perfectly strict, hence the observation of both $g_\parallel$ and $g_\perp$ in **Figure 4c**. However, it is still non-zero, which would only reduce the difference in amplitudes of the two terms in Eq. 1. Thus, the ~100 ps and ~2 ns decay components could correspond to τ_c and T_2^*, respectively. Given the large size of **1**, such a relatively long τ_c is not unreasonable. However, further experiments, ideally with systematic tuning of τ_c, would be needed to confirm this hypothesis. Further discussion of potential origins of the biexponential decoherence and contributions from methyl rotors is given in **SI Section S6**.

Conclusions

In this work, we establish $[WO(OR)_4]^-$ as an optically addressable, room-temperature electron spin qubit. By leveraging ES rather than GS OAM, ultrafast spin dynamics become accessible in lower-symmetry, ligand-tunable molecular complexes rather than only purely octahedral inorganic salts. This strategy also offers a practical advantage in replacing Ir with the more abundant W. Lowering coupling between the spin and its environment by moving OAM to the ES extends T_2^* by nearly two orders of magnitude, showing that a structure–function relationship borne out by prior pulse EPR studies extends to the picosecond regime. The resulting robustness of T_2^* to environmental perturbation, together with the ability to selectively detect DC magnetic fields down to 5 mT,

View Article Online
DOI: 10.1039/D6SC04497B

highlights the sensing promise of this platform. Moreover, if T_2^* is indeed T_1-limited, the strong temperature dependence of T_1 suggests a complementary role in all-optical temperature sensing and probing ultrafast vibrational relaxation mechanisms. Finally, immobilization in a polymer matrix removes rotational averaging and provides a free induction decay encoding *g*-anisotropy. To our knowledge, this is the first ultrafast, fully optically detected EPR spectrum reported for a molecular complex. This work, therefore, enables a route to all-optical sensing of magnetic fields, temperature, and molecular spin structure in platforms compatible with both bulk and microscopic samples. Beyond quantum sensing, these results point to an all-optical approach for interrogating paramagnetic species in coordination chemistry, potentially extending magnetic resonance observables into regimes inaccessible to conventional EPR.

Methods

Synthesis

All reactions and sample preparations were performed using air-free Schlenk line or nitrogen glove box procedures. Dry solvents were obtained from a Pure Process Technology Solvent Purification System and then degassed and stored over molecular sieves in the glove box. 2,6-Diisopropylphenol (Thermo Scientific), sodium hexamethyldisilazide (Thermo Scientific), allyltrimethylsilane (Oakwood), 2,6-dimethylphenol (TCI America), and tungsten (VI) chloride (Strem) were used as received without further purification. $[Na(THF)_6][WO(ODipp)_4]$ (**1**) and $WOCl_3(THF)_2$ were synthesized according to established procedures.[12,27]

Sodium 2,6-dimethylphenoxide (NaODmp) was prepared via deprotonation of 2,6-dimethylphenol (HODmp) with sodium hexamethyldisilazide (NaHMDS) in the glove box. In a 20 mL scintillation vial, 500 mg HODmp (4.09 mmol) was dissolved in 2 mL Et_2O (solution A). In a separate vial, 790 mg (4.29 mmol) NaHMDS was dissolved in 5 mL Et_2O (solution B). Both solutions were then frozen in the glove box cold well (77 K). Upon thawing, B was added dropwise to A while stirring. After stirring for another 30 minutes, the suspension was filtered, washed with hexanes (≈10 mL), and dried to yield a white powder (292 mg, 50%). 1H NMR (400 MHz, CD_3CN) δ 6.72 (doublet, 2H, meta-CH), δ 6.00 (triplet, 1H, para-CH), 2.03 (singlet, 6H, methyl CH3).

$[Na(THF)_4][WO(ODmp)_4]$ (**2**) was prepared in the glove box by reacting 1 eq. $WOCl_3(THF)_2$ with 4.5 eq. NaODmp in THF. In a 20 mL scintillation vial, 51.3 mg (0.113 mmol) $WOCl_3(THF)_2$ was dissolved in 4 mL THF (solution A). In a separate vial, 74.7 mg (0.519 mmol) NaODmp was dissolved in 3 mL THF (solution B). Both solutions were then frozen in the glove box cold well (77 K). Immediately upon thawing, B was added dropwise to A while stirring. After stirring for another 30 minutes, the reaction solution was passed through a syringe filter (0.2 μm pores). The solution was then concentrated under vacuum to ≈4 mL and placed in the glove box freezer (-40 °C) overnight, yielding blue crystals (30 mg, 27%).

Polymer Film Preparation

A 50 mg/mL poly(methyl methacrylate) stock solution was prepared in the glove box by dissolving 118 mg PMMA (Beantown Chemical) in 2.36 mL MeCN and stirring overnight. An 11 mM solution of **1** was then prepared by dissolving 7.5 mg in 500 μL of the PMMA stock. Films were prepared from this solution via drop-casting on 1x1 cm glass slides (12 drops each). Immediately after drop-casting, the slides were covered with a mason jar to ensure slow evaporation. After 3 hours, transparent blue films were obtained and transferred to the glovebox freezer (-40 °C) for storage. For TRFE/R measurements, films were mounted in an airtight cryostat (Oxford Instruments MicrostatHe), removed from the box, and placed along the path of the laser while pulling vacuum on the cryostat to minimize air exposure. For CW and pulse EPR experiments, films were cut into thin strips and placed in a standard X-band EPR tube. To preserve a nitrogen atmosphere, a plug of vacuum grease was inserted at the upper end of the tube before removing it from the glove box.

X-Ray Crystallography

Low-temperature diffraction data (ϕ-and ω-scans) were collected on a Bruker AXS D8 VENTURE KAPPA diffractometer coupled to a PHOTON II CPAD detector with Mo K_α radiation (λ = 0.71073 Å) from an IμS micro-source for the structure of compound V26039 (CSD 2550952). The structure was solved by direct methods using SHELXS3 and refined against F2 on all data by full-matrix least squares with SHELXL-20194 using established refinement techniques.[28–30] All non-hydrogen atoms were refined anisotropically. All hydrogen atoms were included into the model at geometrically calculated positions and refined using a riding model. The isotropic displacement parameters of all hydrogen atoms were fixed to 1.2 times the U value of the atoms they are linked to (1.5 times for methyl groups). All disordered atoms were refined with the help of similarity restraints on the 1,2- and 1,3-distances and displacement parameters as well as enhanced rigid bond restraints for anisotropic displacement parameters.

$[Na(THF)_4][WO(ODmp)_4]$ (CSD 2550952, data block V26039) crystallizes in the tetragonal space group P4/ncc with a quarter of a molecule in the asymmetric unit. The highest electron density maximum is located on the 4-fold rotation axis in a chemically unreasonable location and was not refined.

View Article Online
DOI: 10.1039/D6SC04497B

EPR Spectroscopy

X-band continuous-wave (CW) EPR spectra were collected using a Bruker EMX spectrometer with Bruker Xenon software. All spectra were recorded at a microwave power of 0.14 mW (below the power saturation threshold) and with a modulation amplitude of 2 Gauss. All samples were measured at 77 K using a liquid nitrogen immersion dewar. Spin Hamiltonian fits (**Table S1**) were performed using the EasySpin *pepper* and *esfit* functions in MATLAB.

X-band pulse EPR measurements were collected using a Bruker ELEXSYS E580 EPR spectrometer fitted with a Bruker MD4 resonator. Liquid-helium temperature control was achieved with an Oxford Instruments Mercury ITC temperature controller alongside a CF935 flow cryostat. T_m measurements (**Table S5, S6, S7**) were obtained from the two-pulse Hahn-echo sequence (π/2–τ–π–τ–echo), in which the dephasing time τ was varied. Inversion-recovery measurements of T_1 **(Table S2, S3, S4)** utilized a (π–t–π/2–τ–π–τ–echo) sequence, in which the relaxation time *t* was varied while holding τ constant. The duration of all π/2 pulses was 8 ns, while that of all π pulses was 16 ns. The Hahn-echo decay and inversion recovery measurements were collected using two-step and four-step phase cycling, respectively. At each temperature point, the video gain was optimized. The Hahn-echo decay and inversion recovery data were fit to monoexponential (Eq. 2) and stretched exponential (Eq. 3) functions, respectively. For frozen solution samples, Hahn echo decays were fit to 2τ>800 ns to avoid artifacts from intense proton ESEEM features at low time delays.

$$I = Ae^{\left[-\left(\frac{2\tau}{T_m}\right)\right]} + I_0 \quad \text{(Eq. 2)}$$

$$I = Ae^{\left[-\left(\frac{t}{T_1}\right)^{\beta}\right]} + I_0 \quad \text{(Eq. 3)}$$

Static Optical Spectroscopy

For all solution-phase optical measurements, the sample was held in an airtight quartz cuvette with 2 mm path length, filled under a nitrogen atmosphere. For the TRFE on the thin film, the sample was placed in an optical cryostat under a nitrogen atmosphere and then held under active vacuum over the course of the measurement. All measurements were carried out with the samples at room temperature.

Solution phase absorbance spectra were carried out using a Cary-5000 spectrophotometer. The UV-vis absorption of the film was recorded with a StellarNet fiber-optic spectrophotometer within the glove box.

MCD spectra on solutions were measured using a JASCO J-1700 circular dichroism spectrometer, equipped with a 1.4 T permanent magnet, again using a 2 mm path length cuvette. Circular dichroism spectra were collected for both parallel and antiparallel field directions, then subtracted and halved to leave only the MCD.

Time-Resolved Optical Spectroscopy

Full experimental details regarding the ultrafast setup are given in reference 7 but are briefly described here. All transient measurements proceeded using the same Coherent Astrella fs laser system, which produced ~35 fs pulses centered on 800 nm. Half the pulse power was used to pump an optical parametric amplifier (OPA, Coherent OPerA Solo) to generate pulses centered between 680 – 700 nm. These were used as the pump pulses, and the remaining fundamental was used as the probe, where a moveable retroreflector introduces a time delay in the probe relative to the pump. No difference was observed in TRFE between 680 and 700 nm pump (**Figure S47**), and pulses centered on the two have significant overlap given the broad spectral width of the OPA output. Thus, these are used interchangeably throughout this article.

For TRFE/R, a supercontinuum was generated by focusing the heavily attenuated probe into a 2 mm sapphire crystal. After recollimation, the remaining 800 nm was removed by a 750 nm short-pass filter. From here the probe pulses were focused via a spherical mirror onto the sample and linearly polarized. After the sample, the transmitted and recollimated probe beam entered the balanced detection scheme. This consisted of either a half-wave plate (TRFR) or both half- and quarter-wave plates (TRFE), a Wollaston prism and a pair of photodiodes. The difference in intensity of the two photodiodes—measured with a lock-in amplifier—was proportional to the degree of polarization change in the probe. To select a particular probe wavelength, a 40 nm wide bandpass filter centered on the desired wavelength was placed immediately after the waveplates. The pump pulse was attenuated, chopped to remove every third pulse and circularly polarized by a photoelastic modulator (PEM) before being focused onto the sample. The sample itself was placed in the room-temperature bore of a superconducting magnet, allowing us to apply transverse fields up to 5 T. Unless noted otherwise, all solution-phase TRFE/R was carried out in THF at 11 mM using 1.1 μJ pump and 550 nm probe. All TRFE on the polymer films used 1.6 μJ pump and 550 nm probe. Traces are normalized to 10 ps to aid comparison.

For TA, the pump and probe lines detailed above were passed into an Ultrafast Systems Helios TA Spectrometer. The 800 nm probe generated a supercontinuum in CaF_2, the spectrum of which was measured before and after the sample with CCD array spectrometers. The pump beam was chopped, attenuated, and depolarized

before focusing onto the sample. A custom MATLAB script was used to perform chirp corrections, plotting, and global fitting of the data to a multi-exponential model.

Author Contributions
ES & JPA collected and analyzed the data. All authors contributed towards experimental design and writing.

Conflicts of Interest
There are no conflicts to declare.

Data Availability
Data supporting this article – including additional CW and pulse EPR spectra, TRFE decay traces, and transient absorption measurements – have been included as part of the Supplementary Information. Crystallographic information for **2** has been uploaded to the CSD under deposition number 2550952. Raw data files are available from the corresponding author upon reasonable request.

Acknowledgements
The authors acknowledge Dr. Paul H. Oyala for assistance with EPR instrumentation. They also acknowledge the X-ray Crystallography Facility in the Beckman Institute at Caltech and the Dow Next Generation Instrumentation Grant for X-ray structure collection, as well as Dr. Michael Takase for crystallographic service. E.S. is funded in part by the Gordon and Betty Moore Foundation. J.P.A. acknowledges support from a National Science Foundation Graduate Research Fellowship under Grant No. 2139433. Financial support from an Alfred. P. Sloan Research Fellowship Award (2025-24315) is gratefully acknowledged.

References
1. Bayliss, S. L., Laorenza, D. W., Mintun, P. J., Kovos, B. D., Freedman, D. E., & Awschalom, D. D. Optically addressable molecular spins for quantum information processing. *Science*, 2020, **370**, 1309–1312.
2. Atzori, M., Tesi, L., Morra, E., Chiesa, M., Sorace, L., & Sessoli, R. Room-Temperature Quantum Coherence and Rabi Oscillations in Vanadyl Phthalocyanine: Toward Multifunctional Molecular Spin Qubits. *J. Am. Chem. Soc.*, 2016, **138**, 2154–2157.
3. Gorgon, S., Lv, K., Grüne, J., Drummond, B. H., Myers, W. K., Londi, G., Ricci, G., Valverde, D., Tonnelé, C., Murto, P., Romanov, A. S., Casanova, D., Dyakonov, V., Sperlich, A., Beljonne, D., Olivier, Y., Li, F., Friend, R. H., & Evans, E. W. Reversible spin-optical interface in luminescent organic radicals. *Nature*, 2023, **620**, 538–544.
4. Wasielewski, M. R., Forbes, M. D. E., Frank, N. L., Kowalski, K., Scholes, G. D., Yuen-Zhou, J., Baldo, M. A., Freedman, D. E., Goldsmith, R. H., Goodson, T., Kirk, M. L., McCusker, J. K., Ogilvie, J. P., Shultz, D. A., Stoll, S., & Whaley, K. B. Exploiting chemistry and molecular systems for quantum information science. *Nat Rev Chem*, 2020, **4**, 490–504.
5. Degen, C. L., Reinhard, F. & Cappellaro, P. Quantum sensing. *Rev. Mod. Phys.*, 2017, **89**, 035002.
6. Schirhagl, R., Chang, K., Loretz, M. & Degen, C. L. Nitrogen-Vacancy Centers in Diamond: Nanoscale Sensors for Physics and Biology. *Annual Review of Physical Chemistry*, 2014, **65**, 83–105.
7. Sutcliffe, E., Kazmierczak, N. P. & Hadt, R. G. Ultrafast all-optical coherence of molecular electron spins in room-temperature water solution. *Science*, 2024, **386**, 888–892.
8. Sutcliffe, E., Rothbaum, J. O., Aalto, J. P., Whiteside, J. C. & Hadt, R. G. Prolonging All-Optical Molecular Electron Spin Coherence in the Tissue Transparency Window. *J. Am. Chem. Soc.*, 2025, **147**, 34244–34248.
9. Kazmierczak, N. P., Xia, K. T., Sutcliffe, E., Aalto, J. P. & Hadt, R. G. A Spectrochemical Series for Electron Spin Relaxation. *J. Am. Chem. Soc.*, 2025, **147**, 2849–2859.
10. Espinosa, M. R., Guerrero, F., Kazmierczak, N. P., Oyala, P. H., Hong, A., Hadt, R. G., & Agapie, T. Slow Electron Spin Relaxation at Ambient Temperatures with Copper Coordinated by a Rigid Macrocyclic Ligand. *J. Am. Chem. Soc.*, 2025, **147**, 14036–14042.
11. Ariciu, A.-M., Woen, D. H., Huh, D. N., Nodaraki, L. E., Kostopoulos, A. K., Goodwin, C. A. P., Chilton, N. F., McInnes, E. J. L., Winpenny, R. E. P., Evans, W. J., & Tuna, F. Engineering electronic structure to prolong relaxation times in molecular qubits by minimising orbital angular momentum. *Nat Commun*, 2019, **10**, 3330.
12. Ramsier, I. E., Mandato, A., Saxena, S. & Transue, W. J. Molecular Design for Optically Induced Magnetization: Targeting Excited State Orbital Degeneracy in Tungsten(V) Complexes. *J. Am. Chem. Soc.*, 2025, **147**, 18424–18430.
13. Bendix, J., Brorson, M. & Schaffer, C. E. Accurate empirical spin-orbit coupling parameters ζ_{nd} for gaseous nd^q transition metal ions. The parametrical multiplet term model. *Inorg. Chem.*, 1993, **32**, 2838–2849.

14. Neese, F. & Solomon, E. I. Calculation of Zero-Field Splittings, g-Values, and the Relativistic Nephelauxetic Effect in Transition Metal Complexes. Application to High-Spin Ferric Complexes. *Inorg. Chem.*, 1998, **37**, 6568–6582.
15. Neese, F. & Solomon, E. I. MCD *C*-Term Signs, Saturation Behavior, and Determination of Band Polarizations in Randomly Oriented Systems with Spin $S \geq {}^1/_2$. Applications to $S = {}^1/_2$ and $S = {}^5/_2$. *Inorg. Chem.*, 1999, **38**, 1847–1865.
16. Buch, C. D., Kundu, K., Marbey, J. J., van Tol, J., Weihe, H., Hill, S., & Piligkos, S. Spin–Lattice Relaxation Decoherence Suppression in Vanishing Orbital Angular Momentum Qubits. *J. Am. Chem. Soc.*, 2022, **144**, 17597–17603.
17. Sato, H., Kathirvelu, V., Fielding, A., Blinco, J. P., Micallef, A. S., Bottle, S. E., Eaton, S. S., & Eaton, G. R. Impact of molecular size on electron spin relaxation rates of nitroxyl radicals in glassy solvents between 100 and 300 K. *Molecular Physics*, 2007, **105**, 2137–2151.
18. Spychal, T., Lath, D. & Berek, D. Thermodynamic and hydrodynamic properties of the the systems polymer–tetrahydrofuran–water: 1. Solution properties of polystyrene. *Polymer*, 1979, **20**, 437–442.
19. Yu, C.-J., Graham, M. J., Zadrozny, J. M., Niklas, J., Krzyaniak, M. D., Wasielewski, M. R., Poluektov, O. G., & Freedman, D. E. Long Coherence Times in Nuclear Spin-Free Vanadyl Qubits. *J. Am. Chem. Soc.*, 2016, **138**, 14678–14685.
20. Jahn, S. M., Stowell, R. K. & Stoll, S. The contribution of methyl groups to electron spin decoherence of nitroxides in glassy matrices. *J. Chem. Phys.*, 2024, **161**, 174119.
21. Stoll, S. & Schweiger, A. EasySpin, a comprehensive software package for spectral simulation and analysis in EPR. *Journal of Magnetic Resonance*, 2006, **178**, 42–55.
22. Kozuki, K., Nagashima, T. & Hangyo, M. Measurement of electron paramagnetic resonance using terahertz time-domain spectroscopy. *Opt. Express, OE*, 2011, **19**, 24950–24956.
23. Abrahams, G. *et al.* Quantum spin resonance in engineered proteins for multimodal sensing. *Nature*, 2026, **649**, 1172–1179.
24. Furue, S., Kohmoto, T., Kunitomo, M. & Fukuda, Y. Optical induction of magnetization and observation of fast spin dynamics in aqueous solutions of copper ions. *Physics Letters A*, 2005, **345**, 415–422.
25. Henry, E. R., Eaton, W. A. & Hochstrasser, R. M. Molecular dynamics simulations of cooling in laser-excited heme proteins. *Proc. Natl. Acad. Sci. U.S.A.*, 1986, **83**, 8982–8986.
26. Baumann, T., Hauf, M., Schildhauer, F., Eberl, K. B., Durkin, P. M., Deniz, E., Löffler, J. G., Acevedo-Rocha, C. G., Jaric, J., Martins, B. M., Dobbek, H., Bredenbeck, J., & Budisa, N. Site-Resolved Observation of Vibrational Energy Transfer Using a Genetically Encoded Ultrafast Heater. *Angew Chem Int Ed*, 2019, **58**, 2899–2903.
27. Persson, C. & Andersson, C. Reduction of tungsten(VI) and molybdenum(V) by allyltrimethylsilane and cyclopentene. Simple high yield syntheses of $MoCl_4(OEt_2)_2$, $MoCl_4$(dme), $WCl_4(thf)_2$, WCl_4(dme) and $WOCl_3(thf)_2$. *Inorganica Chimica Acta*, 1993, **203**, 235–238.
28. Zecevic, A.; Eaton, G. R.; Eaton, S. S.; and Lindgren, M. Dephasing of electron spin echoes for nitroxyl radicals in glassy solvents by non-methyl and methyl protons. *Molecular Physics*, 1998, **95**, 1255-1263.
29. Eaton, G. R. and Eaton, S. S. Solvent and temperature dependence of spin echo dephasing for chromium(V) and vanadyl complexes in glassy solution. *Journal of Magnetic Resonance*, 1999, **136**, 63-68.
30. Sheldrick, G. M. Phase annealing in SHELX-90: direct methods for larger structures. *Acta Cryst A*, 1990, **46**, 467–473.
31. Sheldrick, G. M. Crystal structure refinement with SHELXL. *Acta Cryst C*, 2015, **71**, 3–8.
32. Müller, P. Practical suggestions for better crystal structures. *Crystallography Reviews*, 2009, **15**, 57–83.

View Article Online
DOI: 10.1039/D6SC04497B

Data Availability

Data supporting this article – including additional CW and pulse EPR spectra, TRFE decay traces, and transient absorption measurements – have been included as part of the Supplementary Information. Crystallographic information for **2** has been uploaded to the CSD under deposition number 2550952. Raw data files are available from the corresponding author upon reasonable request.